symmetry

MDPI

Article

A Novel Symmetrical Peak Fitting Method Based on Improved WOA Algorithm for the Analysis of Microchip Electrophoresis Signals

Wenhe He [1,2], Jianjiao Wang [3], Yaping Liu [3], Zhipeng Qin [3], Cuimin Sun [4], Hui You [1,3,*], Xiangfu Wei [3] and Ying Liu [1,5]

[1] Key Laboratory of Disaster Prevention and Structural Safety of Ministry of Education, Guangxi University, Nanning 530004, China
[2] School of Electrical Engineering, Guangxi University, Nanning 530004, China
[3] School of Mechanical Engineering, Guangxi University, Nanning 530004, China
[4] School of Computer, Electronics and Information, Guangxi University, Nanning 530004, China
[5] Guangxi Key Laboratory of Disaster Prevention and Engineering Safety, Guangxi University, Nanning 530004, China
* Correspondence: usmlhy@iim.ac.cn

Abstract: The problem of overlapping peaks has been a challenge in microchip electrophoresis (ME) signal analysis. However, traditional peak fitting algorithms have difficulty analyzing overlapping peaks due to the high dependence on the starting point. In this study, we propose a symmetrical peak fitting method named the tent-mapped whale optimization algorithm and Levenberg–Marquardt (TWOALM), which combines a whale optimization algorithm (WOA) improved by one of the most commonly used chaotic maps, the tent map and the Levenberg–Marquardt (LM) algorithm. Specifically, we first derive the fitted model for the overlapping peaks, showing that it is separable nonlinear least squares, significantly reducing the number of parameters to be optimized. Second, we integrate the tent map into the WOA, which improves the convergence speed of the peak fitting algorithm. Finally, we propose an efficient peak-fitting algorithm that combines the improved WOA and LM. The advantage of the proposed algorithm is that it is significantly faster than WOA and significantly more accurate than the LM algorithm. The results of fitting the synthetic peaks and ME signals showed that the combination of the chaotic map-based WOA algorithm and the LM algorithm can significantly improve the peak fitting performance and provide an effective solution for the analysis of overlapping peaks.

Keywords: whale optimization algorithm; chaotic map; Levenberg–Marquardt algorithm; peak fitting method; microchip electrophoresis; ion signal analysis

Citation: He, W.; Wang, J.; Liu, Y.; Qin, Z.; Sun, C.; You, H.; Wei, X.; Liu, Y. A Novel Symmetrical Peak Fitting Method Based on Improved WOA Algorithm for the Analysis of Microchip Electrophoresis Signals. *Symmetry* **2022**, *14*, 2603. https://doi.org/10.3390/sym14122603

Academic Editor: Adam Glowacz

Received: 10 November 2022
Accepted: 5 December 2022
Published: 8 December 2022

1. Introduction

Microchip electrophoresis (ME) has been widely applied in environmental analysis due to its unique advantages [1]. However, similar to other separation techniques, the ME system also has the problem of overlapping peaks [2,3], which becomes a challenge for quantitative analysis.

For the overlapping peak problem, a variety of approaches have been proposed. These commonly used methods include the Kalman filter [4], multiple linear regression [5], reinforcement learning [6], artificial neural networks [7], and continuous wavelet transform [8]. Recently, many methods for handling overlapping chromatographic peaks have been proposed, including techniques suitable for processing single-channel data [9], such as iterative curve fitting [10], power law [11], and derivative method [12]. Among these methods, the iterative curve fitting method is more suitable for the extraction of overlapping peak areas [9].

Since the peaks are special curves, the peak fitting can be considered a nonlinear least squares problem. The most common method for solving this problem is the Levenberg–Marquardt (LM) algorithm [13], which takes the entire data as the fitting object and has the characteristics of fast local convergence. However, since the LM algorithm is an iterative local optimization algorithm, its optimization results are heavily dependent on the starting point [14–16]. Therefore, a suitable starting point for LM needs to be calculated using an algorithm with global optimization capability.

Recently, Li et al. [17] used the particle swarm optimization (PSO) algorithm for curve fitting, which expanded the application of swarm intelligence optimization algorithms. Among the many swarm intelligence optimization algorithms, the whale optimization algorithm (WOA) [18] balances exploration and exploitation well and shows a strong global optimization capability. To the knowledge of the authors, there is no related research on applying the WOA algorithm to peak fitting.

In summary, we combine the improved WOA algorithm with the LM algorithm for the fitting of overlapping peaks in this article. First, the fitted model of the Gaussian peak was derived and specified as separable nonlinear least squares, which effectively reduced the number of parameters to be optimized. Subsequently, the chaos map [19] was integrated into the WOA to improve the peak fitting performance. The results of fitting to the synthetic peaks showed that the convergence speed of WOA based on the tent map was significantly improved. Finally, a peak fitting algorithm based on improved WOA and LM was proposed and evaluated using synthetic peaks and ME signals.

The original contributions of this article are as follows:

First, to analyze the parameters to be optimized, we derived a Gaussian peak fitting model, showing that it is a separable nonlinear least squares problem, which facilitates the coding of individuals. Secondly, to improve the performance of the WOA, an improved WOA algorithm based on tent mapping was proposed. The proposed algorithm improved the convergence speed of the WOA without increasing the time complexity. Finally, aiming at the quantitative analysis of overlapping peaks, a peak fitting algorithm combining the improved WOA and the LM was proposed, which can effectively solve the problem that the LM algorithm relies heavily on the starting point. The method can fit overlapping peaks in microchip electrophoresis and has a high application value.

Compared with published methods for overlapping peak analysis (Refs. [4–8]), our algorithm is more suitable for analyzing the overlapping microchip electrophoresis ion peaks. In addition, the proposed algorithm is computationally efficient and has a broader application prospect than the existing single-channel signal analysis methods (Refs. [11,12]). Our algorithm has a higher fitting accuracy and shorter computation time than the LM algorithm (Ref. [13]) and WOA algorithm (Ref. [18]), respectively.

The following sections are organized as follows: in Section 2, the derivation of the fitting model, the theory of the WOA, LM, and chaotic maps, and the description of the proposed algorithm, are introduced. In Section 3, the proposed method is introduced. Section 4 describes the acquisition process of simulation data and electrophoresis data. In Section 5, synthetic data and experimental data are used to verify the performance of the proposed algorithm. Finally, the conclusion is given in Section 6.

2. Related Work

2.1. Derivation of Peak Fitting Model

In peak fitting, analysts generally consider that the detected signal is the superposition of multiple independent components [20]. In other words, the fitting object is the addition of multiple independent peaks. In addition, as one of the most commonly used peak shapes, the Gaussian function has shown its powerful ability for the description of peak shape data [21] and the analysis of signals, such as spectroscopy [22], chromatography [23], mass spectrometry [24], magnetic eddy current [25], and voltammetry [26]. The structure of

voltage signals obtained by ion sample detection using a microchip electrophoresis device is assumed to be the superposition of Gaussians

$$y(\boldsymbol{t}) = \sum_{i=1}^{N} h_i \times e^{-\left(\frac{t-p_i}{w_i}\right)^2 \times ln16}, \tag{1}$$

where $\boldsymbol{t}$ is the time variable, N is the number of component peaks, i.e., the number of separated peaks, while the h_i, p_i, and w_i are the height, position, and width of the i-th Gaussian peak, respectively.

Equation (1) shows that h_i is a linear parameter, and both p_i and w_i are non-linear parameters. Considering the Gaussian function as a special exponential function, then Equation (1) is a linear combination of N exponential functions. In other words, Equation (1) is a linear combination of multiple nonlinear functions with multiple parameters. Hence, according to Reference [27], Equation (1) is a separable nonlinear least squares problem. For convenience, we rewrite Equation (1) as

$$y(t; \boldsymbol{h}, \boldsymbol{p}, \boldsymbol{w}) = \boldsymbol{h} * \boldsymbol{X}^{\mathrm{T}}, \tag{2}$$

where $*$ means the inner product, T is the matrix (vector) transpose, $\boldsymbol{h}$ is the linear parameter vector, $\boldsymbol{X}$ is the function of nonlinear parameter vectors $\boldsymbol{p}$ and $\boldsymbol{w}$. The descriptions of vectors $\boldsymbol{h}$, $\boldsymbol{p}$, and $\boldsymbol{w}$ are

$$\boldsymbol{h} = [h_1, h_2, \ldots, h_N], \tag{3}$$

$$\boldsymbol{p} = [p_1, p_2, \ldots, p_N], \tag{4}$$

$$\boldsymbol{w} = [w_1, w_2, \ldots, w_N]. \tag{5}$$

For the peak fitting problems, the k-th element of the fitting residual can be expressed as

$$r_k(\boldsymbol{h}, \boldsymbol{p}, \boldsymbol{w}) = y^*(t_k) - y(t_k; \boldsymbol{h}, \boldsymbol{p}, \boldsymbol{w}), \tag{6}$$

where y^* is the measured signal.

The residual vector of peak fitting is

$$\boldsymbol{r}(\boldsymbol{h}, \boldsymbol{p}, \boldsymbol{w}) = [r_1(\boldsymbol{h}, \boldsymbol{p}, \boldsymbol{w}), \ldots, r_M(\boldsymbol{h}, \boldsymbol{p}, \boldsymbol{w})], \tag{7}$$

where M is the number of data points in the measured signal.

According to the principle of least squares, the parameters $\boldsymbol{h}$, $\boldsymbol{p}$, and $\boldsymbol{w}$ are determined by minimizing the Euclidean norm of the $\boldsymbol{r}$ vector

$$\|\boldsymbol{r}(\boldsymbol{h}, \boldsymbol{p}, \boldsymbol{w})\|_2 = \|\boldsymbol{y}^* - \boldsymbol{h} * \boldsymbol{x}^{\boldsymbol{T}}\|_2. \tag{8}$$

Assuming that the nonlinear parameters $\boldsymbol{p}$ and $\boldsymbol{w}$ in Equation (8) have been determined, as discussed later, the parameter $\boldsymbol{h}$ can be obtained by solving linear least squares

$$\boldsymbol{h} = \boldsymbol{y}^* * inv\left(\boldsymbol{x}^T\right), \tag{9}$$

where inv is the inverse of the matrix.

In this article, the fitting error of the algorithm is the root mean square error (RMSE), as follows:

$$RMSE = \frac{\|\boldsymbol{r}(\boldsymbol{h}, \boldsymbol{p}, \boldsymbol{w})\|_2}{\sqrt{M}}. \tag{10}$$

The difficulty of this problem lies in the solution of nonlinear parameters. According to Equation (8), the minimization of the peak fitting error can be regarded as a least squares problem, including linear and nonlinear parts. To solve this problem, the nonlinear parameters ($\boldsymbol{p}$ and $\boldsymbol{w}$) should be determined before calculating the linear parameter ($\boldsymbol{h}$). Although the LM algorithm can determine $\boldsymbol{p}$ and $\boldsymbol{w}$, the LM algorithm is an iterative

gradient algorithm which is highly dependent on the starting point. To find a suitable starting point for LM, the improved WOA algorithm is described in detail in Section 3.

2.2. Theory of WOA, LM, and Chaotic Map

2.2.1. WOA

The WOA algorithm has comprehensive advantages in terms of global optimization capability and convergence and is therefore used to perform peak fitting. The optimization process of the WOA algorithm includes two stages: exploration and exploitation.

In the exploration phase, to improve the global optimization ability, the position updates with the randomly chosen individual and

$$P(k+1) = P^*(k) - C_1 \cdot |C_2 \cdot P^*(k) - P(k)|, \tag{11}$$

where P is the position vector, k means the current iteration, P^* means the position vector of the best individual, and C_1 and C_2 are coefficient vectors described later.

The descriptions of the coefficient vectors C_1 and C_2 are

$$C_1 = 2d \cdot r_1 - d, \tag{12}$$

$$C_2 = 2r_2, \tag{13}$$

respectively, where d decreases linearly from 2 to 0 as the iteration increases, r_1 and r_2 are vectors of random numbers between 0 and 1. It should be noted that Equation (11) is used only when the absolute value of C_1 is greater than or equal to 1.

During the exploitation phase, the position updates according to the target's position or in a spiral fashion with a probability of 50% each

$$P(k+1) = \begin{cases} P^*(k) - C_1 \cdot |C_2 \cdot P^*(k) - P(k)|, & \text{if } p < 0.5 \quad (14) \\ |P^*(k) - P(k)| \cdot e^{bl} \cdot \cos(2\pi l) + \overline{P}(k), & \text{if } p \geq 0.5 \quad (15) \end{cases}$$

where P^* is the position vector of the target (the best solution), the term $|P^*(k) - P(k)|$ means the distance between the current whale and the target, the constant b indicates the shape of the spiral, l is a random number between -1 and 1, p is a uniformly distributed random number in [0,1]. It should be noted that Equation (14) can only be used when the absolute value of C_1 is less than 1.

2.2.2. LM

Due to the optimization ability of the LM algorithm, it has been widely used for data fitting, including mass spectrometry [28], voltammetry [29], chromatography [30], Raman spectroscopy [31], laser-induced breakdown spectroscopy [32], and fiber Bragg grating data [33]. The LM effectively combines the gradient descent method and the Gauss–Newton iteration method and is one of the most widely used optimization algorithms. The key step of the LM algorithm is

$$x(i+1) = x(i) - (H + \lambda diag[H])^{-1} \nabla f(x(i)), \tag{16}$$

where $x = (x_1, x_2, \ldots, x_n)$ is a vector of the parameter to be optimized, is the Hessian matrix evaluated at $x(i)$, λ is the scale coefficient, $diag$ is the diagonal of the matrix, $\nabla f(x(i))$ is the gradient of the objective function f at $x(i)$. It can be seen from Equation (16) that the LM algorithm significantly depends on $x(0)$, which is the starting point.

2.2.3. Chaotic Map

The complex behavior in nonlinear or deterministic systems can be represented by chaotic maps. The randomness and ergodic nature of chaotic maps are widely used for the improvement of swarm intelligence algorithms [19,34–37]. On the one hand, these studies based on chaotic maps have significantly improved the performance of swarm intelligence

algorithms. On the other hand, the convergence speed [38] of the WOA algorithm has room for improvement. Therefore, we are motivated to apply chaotic maps to improve the performance of the WOA algorithm. Tent map and Gauss/mouse map are used in this article, as shown below:

$$u_{i+1} = \begin{cases} \frac{u_i}{0.7}, & u_i < 0.7 \\ \frac{10(1-u_i)}{3}, & u_i \geq 0.7 \end{cases} \quad (17)$$

$$u_{i+1} = \begin{cases} 1, & u_i = 0 \\ \frac{1}{mod(u_i,1)}, & u_i \neq 0 \end{cases} \quad (18)$$

3. Proposed Method

3.1. Improved WOA

To further improve the performance of the WOA algorithm, we replaced the uniformly distributed p in the original WOA algorithm with a chaotic map, as shown in Equations (19) and (20).

$$P(k+1) = \begin{cases} P^*(k) - C_1 \cdot |C_2 \cdot P^*(k) - P(k)|, & \text{if } cmp < 0.5 \quad (19) \\ |P^*(k) - P(k)| \cdot e^{bl} \cdot \cos(2\pi l) + \overline{P}(k), & \text{if } cmp \geq 0.5 \quad (20) \end{cases}$$

where cmp is a chaotic mapped value calculated by Equation (17) or (18). The pseudo-code of the tent map-based WOA algorithm is as Algorithm 1.

Algorithm 1. The pseudo-code of the TWOA

```
Begin
  Initialize the position of each individual;
  Calculate each fitness and find the best optimal individual (P*);
  while t ≤ MaxIter
    for each individual
      Return back the individuals that beyond the boundaries;
      Update the iteration parameters (d, r1, r2, C1, C2, and l);
      Update the tent map probability (cmp) by Equation (17);
      if p < 0.5
        if C1 < 1
          Update the position of the individual by Equation (14);
        else
          Update the position of the individual by Equation (11);
        end
      else
        Update the position of the individual by Equation (15);
      end
    end
    Update P* and t;
  end
  return P*;
End
```

For synthetic peaks, Figure 1 depicts the convergence curves of the WOA fitting algorithm with different chaotic maps. Figure 1 shows that the WOA with a tent map converged faster than the original WOA. In contrast, it can be seen from Figure 1 that the WOA with a Gauss/mouse map failed to effectively improve the convergence speed of the original WOA. Furthermore, most of the tent-mapped WOAs converged around the 20th iteration. This indicates that for peak fitting problems, tent mapping techniques can improve the performance of WOA.

For further comparison, the fitting results of the original WOA, Gauss/mouse-mapped WOA, and tent-mapped WOA are shown in Figures A1–A8 in Appendix A. Figures A1a–A8a

show that for all six sets of synthetic data, the fitting errors of the Gauss/mouse-mapped WOA were larger than those of the other two algorithms. In addition, although the fitting errors of tent-mapped WOA and original WOA were not significantly different for the first three sets of data, the errors of the tent-mapped WOA were lower than those of the original WOA on all six sets of data. Figures A1b–A8b compare the computation time of these three algorithms for six sets of data. For each set of data, the tent-mapped WOA had the fastest computation speed while the original WOA had the longest running time. A comprehensive analysis of the convergence properties (Figure 1) and fitting results (Figures A1–A8) shows that the chaotic mapping technique (tent map) can improve the peak fitting performance of WOA. Therefore, the tent-mapped WOA (TWOA) was used in this work.

To determine the nonlinear parameters in Equation (8), we used the improved WOA algorithm to calculate the starting point for the LM algorithms. To use the TWOA, peak fitting parameters such as $\boldsymbol{h}$, $\boldsymbol{p}$ and $\boldsymbol{w}$ should be coded according to the position vector

$$Pos(k) = [h_1, p_1, w_1, h_2, p_2, w_2, \ldots, h_N, p_N, w_N]. \tag{21}$$

Then the optimal solution $\overline{Pos}$ is found at the end of the WOA iteration, as shown in Equation (22)

$$\overline{Pos} = \left[\overline{h_1}, \overline{p_1}, \overline{w_1}, \overline{h_2}, \overline{p_2}, \overline{w_2}, \ldots, \overline{h_N}, \overline{p_N}, \overline{w_N}\right], \tag{22}$$

which can serve as the starting point of the LM algorithm.

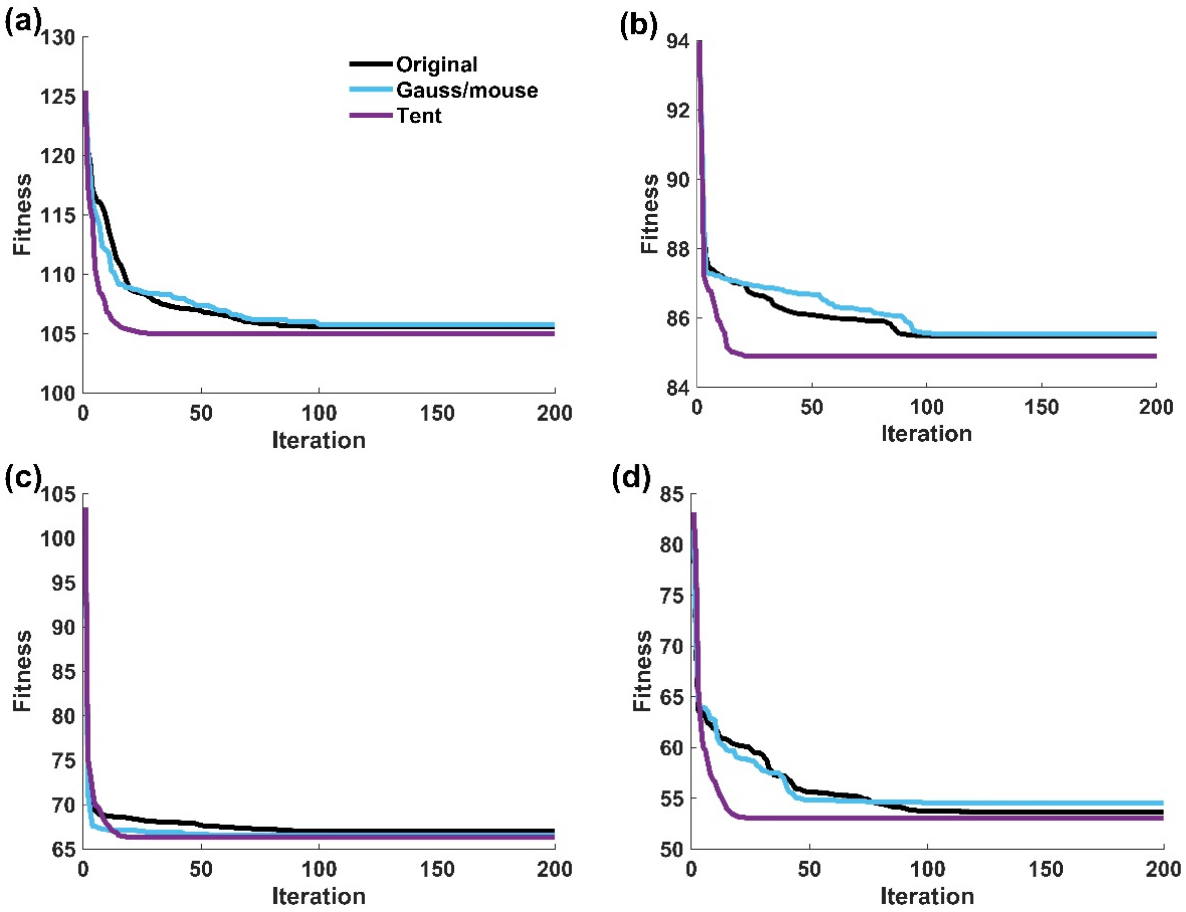

Figure 1. *Cont.*

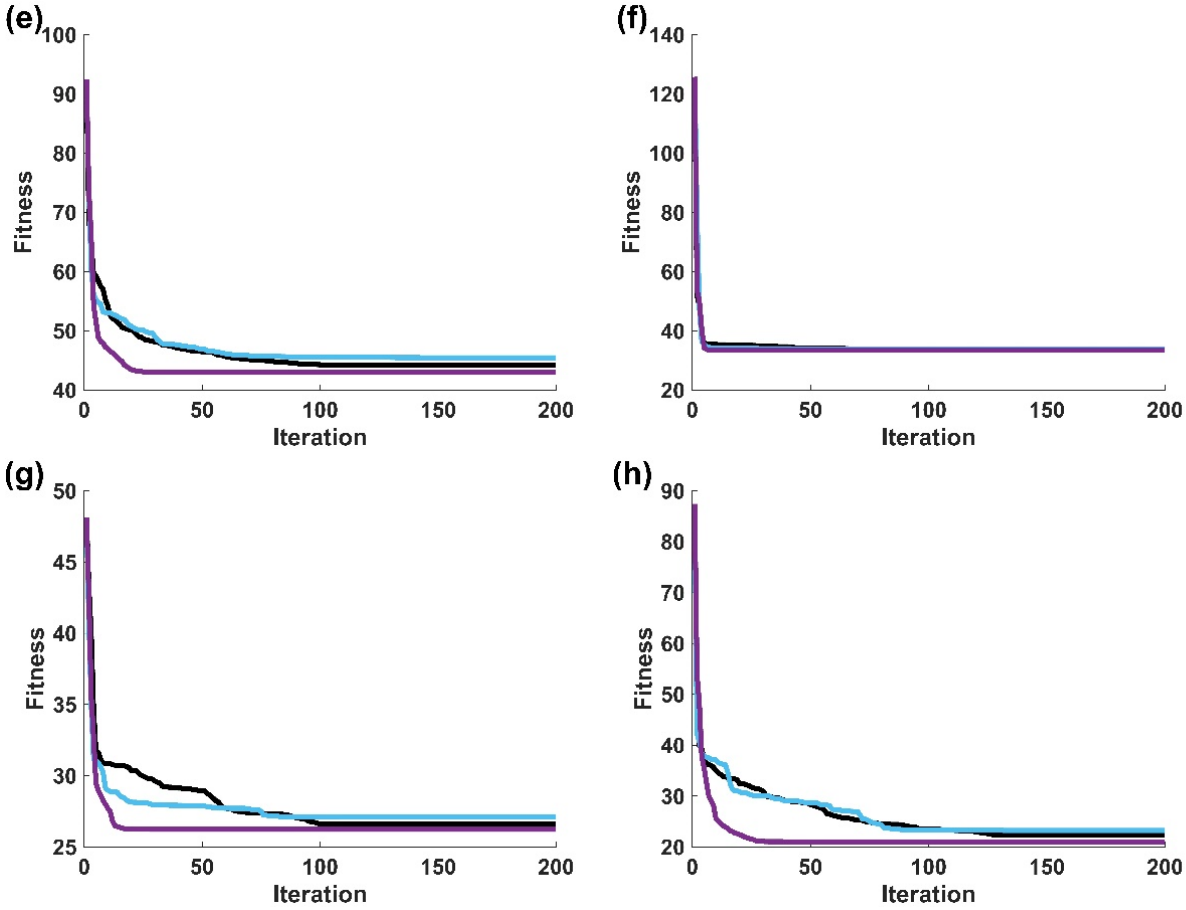

Figure 1. Convergence curves of the WOAs with different chaotic maps. Subfigures (**a**–**h**) are the results of fitting the signals with signal-to-noise ratios of 10, 12, 14, 16, 18, 20, 22, and 24 dB, respectively. The resolution of each pair of synthetic peaks is 0.65.

3.2. Proposed Peak Fitting Method

Figure 2 shows a simplified flowchart of the proposed TWOA-based LM algorithm named TWOALM, and its brief description is as follows:

(1) Input stage, where the microchip electrophoresis signals are preprocessed to be suitable for application in the peak fitting method;

(2) Baseline correction, aims to subtract background information from the signal to facilitate subsequent processing;

(3) Initialization, setting the initial parameters of the TWOA algorithm to achieve global optimization;

(4) TWOA calculation, update the cmp with Equation (17), fit the Gaussian functions to the detected microchip electrophoresis ion signals, and then use the optimal solution as the starting point of the LM algorithm; and,

(5) Based on the starting point obtained from the previous stage, the LM algorithm performs further peak fitting. If the current iteration t is less than the maximum iteration (MaxIter) and the best fitness (BF) is greater than the preset error (SetError), return to the third stage, otherwise, output the result.

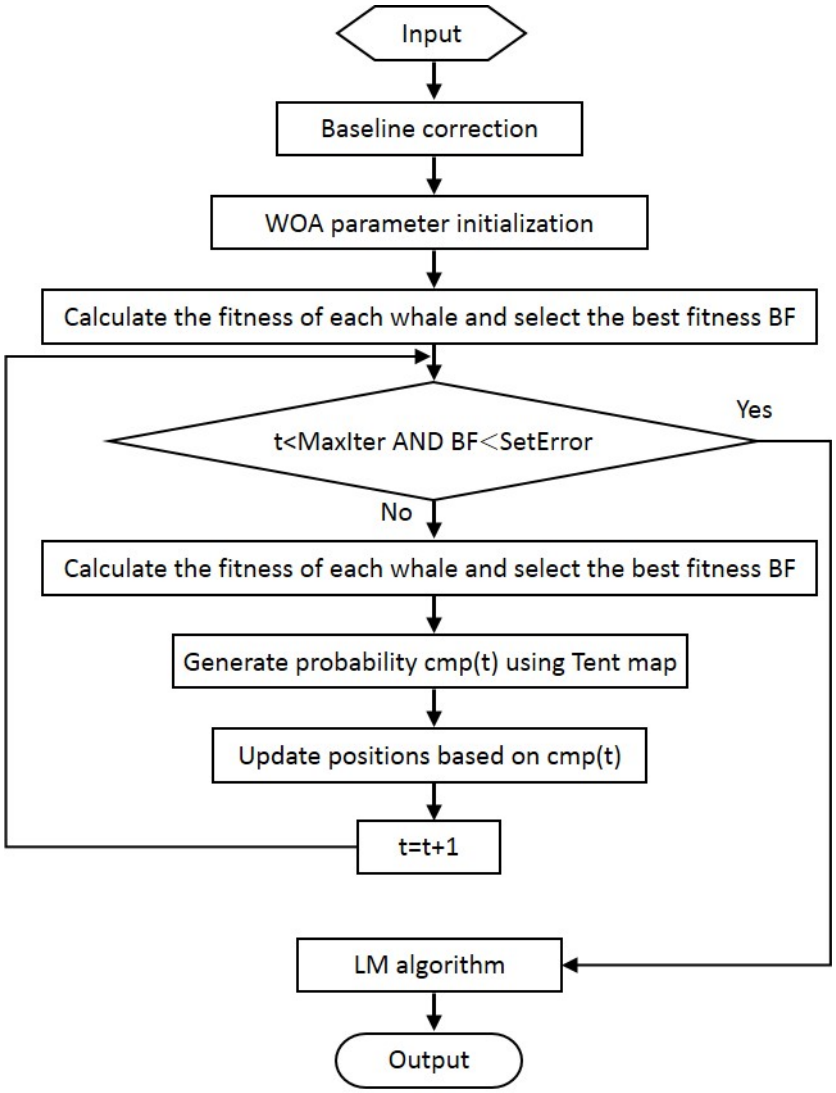

Figure 2. Simplified flow chart of the proposed peak fitting algorithm.

4. Materials and Experiments

4.1. Synthetic Peaks

The synthetic data are the sum of two Gaussian peaks with different parameters

$$Syn1(\boldsymbol{t}) = \sum_{i=1}^{2} h_i \times e^{-\left(\frac{t-p_i}{w_i}\right)^2 \times ln16}, \tag{23}$$

where $Syn1$ means the synthetic data, $\boldsymbol{t}$ is the time variable vector, h_i, p_i, and w_i are the height, position, and width of i-th Gaussian peak, respectively.

Generally, the resolution of two Gaussian peaks [39] can be expressed as

$$R_G = \frac{(p_2 - p_1)}{2(\sigma_1 + \sigma_2)}, \tag{24}$$

where R_G is the resolution, and σ_1 and σ_2 are the standard deviations of the two Gaussian distributions. In addition, it is more practical to use the full width at half maximum ($FWHM$) to describe the width of the peak. For Gaussian distribution [40], the relationship between $FWHM$ and standard deviation is

$$\sigma_i = \frac{FWHM_i}{2\sqrt{\ln 4}}, \tag{25}$$

where the subscript i represents the i-th Gaussian peak. Finally, Equation (24) can be rewritten into a more practical form

$$R_G = \frac{(p_2 - p_1)\sqrt{\ln 4}}{(FWHM_1 + FWHM_2)}. \quad (26)$$

To simulate the real ion signals, eight different levels of white noise were added to the data. Here, the signal-to-noise ratio (SNR) increased by 2 dB from 10 dB to 24 dB. In all these synthetic data, the height of the first peak was set to 1000, and the height of the other peak was set to 500. The $FWHM$ of the two peaks were 200 and 400, respectively. It is important to note that under the same noise level, the value of p_1 was fixed at 800, while the value of p_2 decreased by 30 from 1370 to 110. Therefore, according to Equation (26), there are nine sets of overlapping peaks with different resolutions. The population size of both WOA and TWOA is 500, and the maximum number of iterations is 200. Repeat the calculation 100 times for each set of data, and then calculate the fitting error. The configuration of the personal computer used to perform the simulation results is as follows: the computer performing the calculations has an Intel(R) Xeon(R) Silver 4108 CPU with eight cores (1.80 GHz) and 256 GB memory.

4.2. Reagents and Electrophoresis Experiment

Table 1 shows the details of the solutions used. All analytical-grade reagents were purchased from Macklin (Shanghai, China).

Table 1. Description of the solutions used in this work.

Solution	Property
NH_4^+&K^+	10 mM, stock solutions
Ca^{2+}&Mg^{2+}	10 mM, stock solutions
L-histidine (His)	60 mM stock solution
2-(N-morpholino)-ethanesulfonic acid (MES)	60 mM stock solution
18-Crown-6	20 mM stock solution
Sodium hydroxide	100 mM stock solutions
Deionized water	resistivity 18.2 MΩ·cm

The solutions were prepared using deionized water, which was processed through Cascada I (PALL, Beijing, China). Stock solutions of NH_4^+, K^+, Ca^{2+}, and Mg^{2+} were prepared from their corresponding chloride salts. The stock solutions of His, MES, and 18-Crown-6 (Table 1) were prepared daily. A mixture of these three solutions was the running buffer, which was 20 mM His, 20 mM MES, and 2 mM 18-Crown-6 at pH 6.0. To obtain samples, the sample (high concentration) solutions in Table 1 were diluted with the running buffer. The other experimental conditions were consistent with the work in [41]. Electrophoresis signals were acquired using MAX194 (Maxim Integrated, San Jose, CA, USA) and LABVIEW (National Instruments, Austin, TX, USA).

5. Results and Discussion

5.1. Fitting Results to Synthetic Peaks

Figure 3 shows the fitting errors of LM, TWOA, and TWOALM. It can be seen from Figure 3 that the fitting error of LM was the largest and was significantly greater than that of TWOALM and TWOA. In each case of Figure 3, the fitting error of TWOALM was very close to that of TWOA (the differences were not more than $\pm 10^{-12}$). In addition, the errors of TWOALM (and TWOA) decreased with the increase in SNR. In contrast, the errors of LM did not strictly show this trend in Figure 3d,e,g,h.

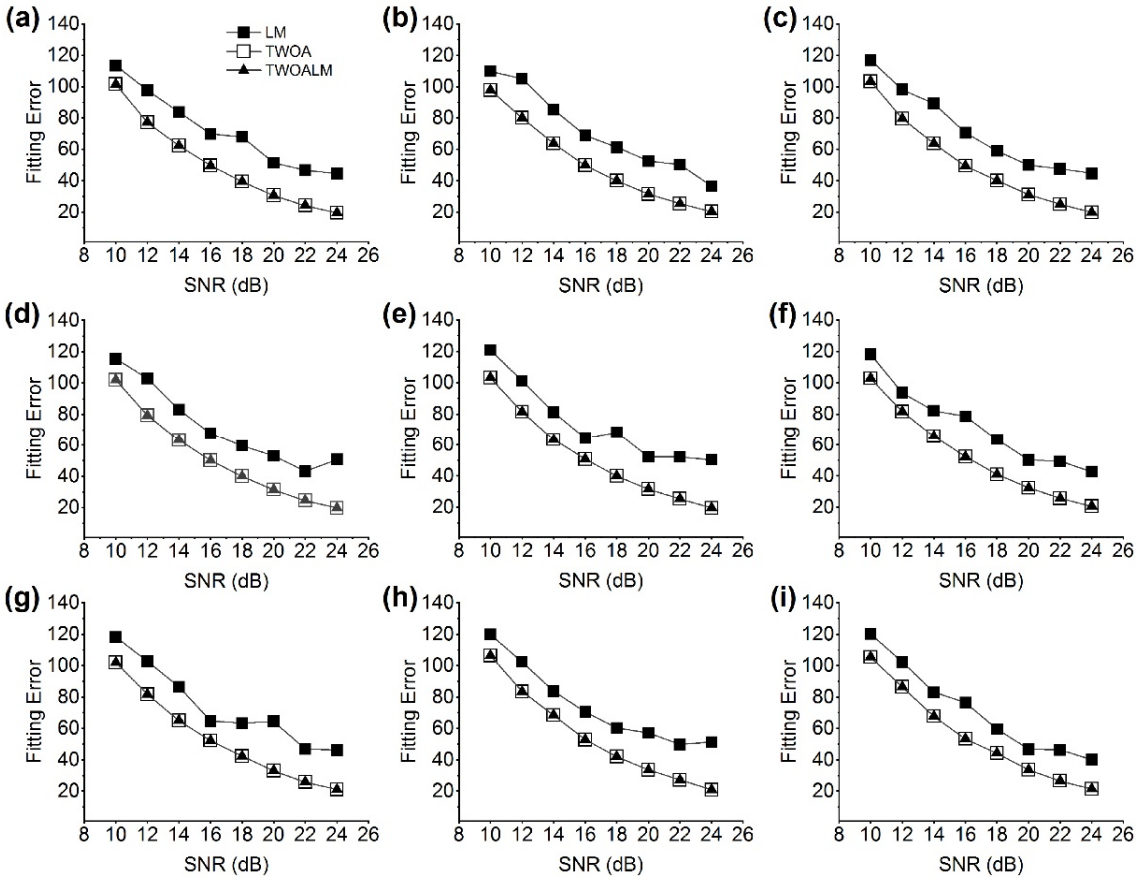

Figure 3. Fitting errors of the LM, TWOA, and TWOALM to different resolution peaks. The resolutions are (**a**) 1.12, (**b**) 1.06, (**c**) 1.00, (**d**) 0.94, (**e**) 0.88, (**f**) 0.82, (**g**) 0.77, (**h**) 0.71, and (**i**) 0.65, respectively. The fitting error is the average of the root mean square error of 100 fittings.

Corresponding to Figure 3, Table 2 shows the calculation time of TWOALM, LM, and TWOA. It can be seen from Table 2 that the calculation time of TWOA was significantly longer than that of LM and TWOALM. For each resolution, the calculation time of TWOA was around 13 s, which is three orders of magnitude larger than that of TWOALM and LM. It is worth noting that the calculation time of TWOALM was the same order of magnitude as that of LM. In most cases, the computer time of TWOALM was greater than that of LM when the resolution was higher than R5. In contrast, when the resolution was below R5, the computer time of TWOALM was smaller than that of LM in most cases. Taking resolution R9 (0.65) as an example, the fitting results in Figure 4 also reflect the excellent performance of the proposed fitting algorithm. Table 3 shows the peak position errors of TWOALM and LM. It can be seen from Table 3 that for each combined peak, the peak position errors (Error1 and Error2) of TWOALM were significantly smaller than those of LM, respectively. For most cases of TWOALM or LM, the position error of peak 1 was less than that of peak 2. More specifically, for the LM algorithm, the position errors of peak 2 were significantly greater than those of peak 1 under the resolutions from R3 to R9. In contrast, the TWOALM algorithm showed this trend only in the resolutions of R1 and R7. Table 3 indicates that the fitting accuracy of TWOALM was higher than that of LM.

To sum up, taking into account the fitting errors (Figures 3 and 4), position errors (Table 3), and calculation time (Table 2), the proposed TWOALM algorithm has the advantages of both TWOA and LM, that is, higher fitting accuracy and faster calculation speed. Furthermore, when the resolution of overlapping peaks is lower than 0.88 (R5), the excellent performance of the proposed algorithm can be better reflected.

Table 2. Calculation time of different algorithms for synthesized peaks. R1 to R9 correspond to peaks of resolutions 1.12, 1.06, 1.00, 0.94, 0.88, 0.82, 0.77, 0.71, and 0.65, respectively. The calculation time is the average of the calculation time of 100 fittings.

Resolution	Algorithm	10 dB	12 dB	14 dB	16 dB	18 dB	20 dB	22 dB	24 dB
R1	TWOALM	0.091	0.074	0.073	0.068	0.065	0.060	0.059	**0.057**
	LM	**0.048**	**0.069**	**0.062**	**0.059**	**0.055**	**0.053**	**0.054**	0.058
	TWOA	13.83	13.60	13.61	13.49	13.32	13.54	14.52	13.52
R2	TWOALM	0.077	0.075	0.071	0.068	**0.059**	**0.059**	**0.056**	0.058
	LM	**0.048**	**0.066**	**0.060**	**0.052**	0.080	0.069	0.056	**0.051**
	TWOA	13.15	13.09	13.09	13.23	13.19	13.20	13.40	13.23
R3	TWOALM	0.094	0.078	0.070	0.061	0.056	0.055	**0.052**	0.052
	LM	**0.054**	**0.066**	**0.056**	**0.055**	**0.048**	**0.046**	0.063	**0.051**
	TWOA	14.49	14.04	13.28	13.18	12.83	13.05	12.89	12.86
R4	TWOALM	0.071	0.062	0.070	0.055	0.052	**0.052**	0.050	**0.047**
	LM	**0.050**	**0.054**	**0.054**	**0.047**	**0.048**	0.064	**0.049**	0.054
	TWOA	12.79	12.91	12.89	12.91	12.85	12.95	12.94	12.94
R5	TWOALM	0.070	**0.066**	0.064	**0.056**	**0.054**	**0.049**	**0.044**	**0.047**
	LM	**0.065**	0.071	**0.056**	0.058	0.055	0.054	0.062	0.062
	TWOA	12.88	12.92	12.87	12.92	12.83	12.88	12.84	12.94
R6	TWOALM	0.063	0.057	0.058	**0.052**	**0.050**	**0.050**	**0.045**	**0.045**
	LM	**0.058**	**0.055**	**0.054**	0.070	0.059	0.061	0.060	0.055
	TWOA	0.077	0.075	0.071	0.068	0.059	0.059	0.056	0.058
R7	TWOALM	**0.061**	**0.052**	**0.054**	**0.049**	**0.048**	**0.044**	**0.040**	**0.040**
	LM	0.064	0.069	0.072	0.051	0.061	0.070	0.061	0.092
	TWOA	13.08	12.96	12.90	12.97	12.85	13.02	12.92	12.86
R8	TWOALM	**0.056**	**0.048**	**0.056**	**0.046**	**0.042**	**0.042**	**0.042**	**0.040**
	LM	0.069	0.088	0.075	0.065	0.058	0.073	0.067	0.083
	TWOA	12.86	12.88	12.81	12.85	12.77	12.91	12.87	12.84
R9	TWOALM	**0.056**	**0.049**	**0.050**	**0.043**	**0.040**	**0.039**	**0.037**	**0.039**
	LM	0.075	0.058	0.065	0.062	0.070	0.055	0.070	0.067
	TWOA	12.80	12.84	12.79	12.79	12.80	12.87	12.78	12.78

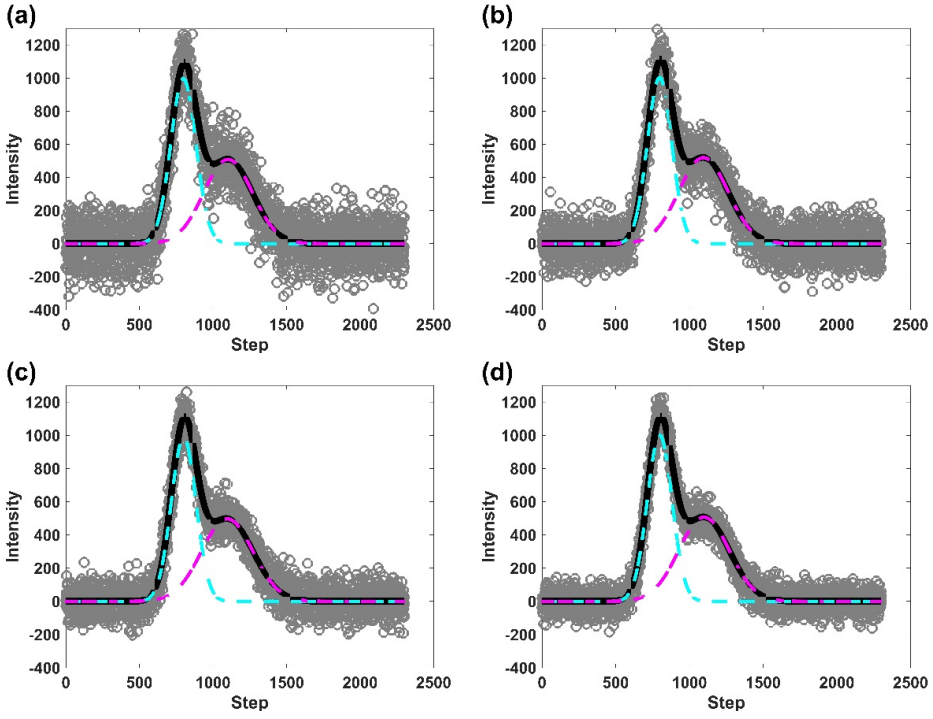

Figure 4. *Cont.*

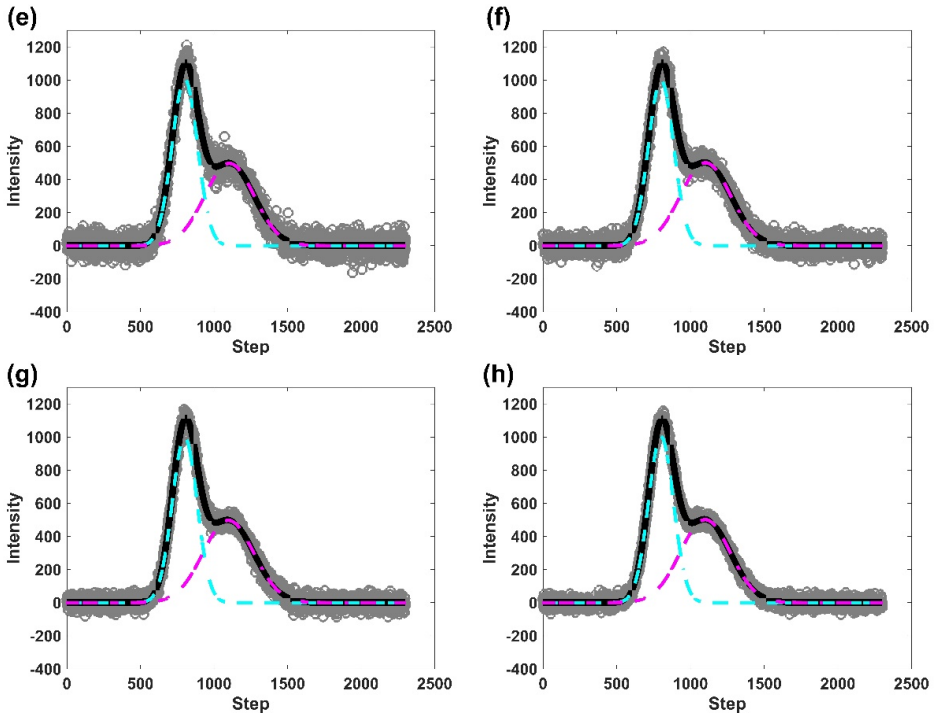

Figure 4. Fitting results of the proposed method to the synthetic peaks with different noise levels. The resolution of each pair of synthetic peaks is 0.65; (**a**–**h**) correspond to eight SNRs, which are 10 dB, 12 dB, 14 dB, 16 dB, 18 dB, 20 dB, 22 dB, and 24 dB, respectively. Gray circles represent the synthetic data; the black solid line is the fitted peak; the two single peaks are plotted with cyan and magenta dashed lines, respectively.

Table 3. Peak position errors of TWOALM and LM for the synthetic peaks with eight signal-to-noise ratios, including position errors of peak 1 (Error1) and peak 2 (Error2). Each error is the absolute value of the mean value of the peak position residuals of 100 fittings. R1 to R9 correspond to peaks of resolutions 1.12, 1.06, 1.00, 0.94, 0.88, 0.82, 0.77, 0.71, and 0.65, respectively.

Resolution	Algorithm		10 dB	12 dB	14 dB	16 dB	18 dB	20 dB	22 dB	24 dB
R1	TWOALM	Error1	0.37	1.13	0.93	0.19	0.03	0.04	0.35	0.02
		Error2	2.38	1.14	2.00	1.78	0.93	1.29	1.14	0.09
	LM	Error1	25.26	14.00	2.29	7.87	1.26	21.97	6.71	14.72
		Error2	95.43	57.97	32.34	40.95	1.18	78.60	45.21	49.18
R2	TWOALM	Error1	2.47	0.15	1.09	0.41	0.03	0.05	0.55	0.22
		Error2	0.20	3.58	1.57	1.50	0.18	0.23	0.24	0.82
	LM	Error1	4.87	4.41	15.84	14.95	5.53	10.76	7.16	30.54
		Error2	27.22	47.72	27.14	42.18	68.47	62.36	37.43	30.29
R3	TWOALM	Error1	0.46	0.84	1.33	1.02	0.00	0.27	0.15	0.46
		Error2	0.34	0.40	0.40	1.81	1.43	0.38	1.13	1.07
	LM	Error1	12.28	22.57	0.34	7.25	3.81	16.04	9.46	3.76
		Error2	64.39	119.47	106.31	93.01	126.93	95.38	80.99	93.81
R4	TWOALM	Error1	0.41	0.09	0.25	1.02	0.54	0.00	0.24	0.42
		Error2	0.20	2.83	3.55	2.12	2.24	0.51	0.01	0.31
	LM	Error1	1.16	10.42	0.38	6.13	13.42	7.05	4.98	1.33
		Error2	67.20	114.28	89.21	135.55	63.58	57.13	102.47	97.05

Table 3. *Cont.*

Resolution	Algorithm		10 dB	12 dB	14 dB	16 dB	18 dB	20 dB	22 dB	24 dB
R5	TWOALM	Error1	1.17	0.78	0.42	0.60	0.11	0.27	0.11	0.00
		Error2	1.52	0.11	1.72	2.87	1.79	0.97	0.07	0.90
	LM	Error1	7.02	15.24	36.10	1.61	13.30	2.80	34.20	0.74
		Error2	136.42	87.49	71.32	156.76	101.51	121.77	104.21	186.19
R6	TWOALM	Error1	3.17	2.76	1.51	0.07	0.55	0.23	0.81	0.10
		Error2	7.63	9.28	1.46	2.20	2.31	0.22	3.13	0.97
	LM	Error1	1.73	29.55	11.17	58.03	13.13	9.94	12.99	14.84
		Error2	182.09	97.30	161.24	121.32	176.53	140.57	199.55	131.12
R7	TWOALM	Error1	1.48	0.02	0.38	0.42	0.24	0.84	0.22	1.78
		Error2	1.86	1.67	0.97	4.59	2.97	2.16	1.96	16.29
	LM	Error1	20.10	29.59	35.12	23.82	14.00	40.29	52.07	44.57
		Error2	235.81	258.37	248.49	215.68	243.54	190.68	165.54	156.71
R8	TWOALM	Error1	4.50	2.20	1.22	12.67	0.76	16.13	27.71	19.07
		Error2	14.45	19.90	3.16	33.68	10.66	44.27	59.23	3.05
	LM	Error1	56.10	24.23	26.26	62.91	53.58	27.57	33.10	27.42
		Error2	330.30	242.44	328.67	295.81	164.69	111.16	263.38	215.16
R9	TWOALM	Error1	0.07	4.59	18.78	28.22	1.63	40.73	11.13	17.16
		Error2	0.80	26.06	2.90	43.38	70.58	33.59	8.17	10.64
	LM	Error1	42.58	23.99	36.55	63.72	35.21	31.12	49.28	46.58
		Error2	228.78	314.41	383.07	219.07	419.76	232.48	292.38	332.37

5.2. Results in the Analysis of Experimental Data

Figure 5 shows the worst-fitting results of the proposed algorithm, the TWOA algorithm, and the LM algorithm on the ME signals of these ionic samples. The residual curve is drawn in the lower part of each figure. Figure 5a–c show the fitting results of the proposed algorithm, TWOA algorithm, and LM algorithm on sample 1 (NH_4^+&K^+), respectively. In addition, the fitting results of these three algorithms on sample 2 (Ca^{2+}&Mg^{2+}) are shown in Figure 5d–f, respectively. Although the complexing agent 18-Crown-6 (Table 1) was added to the running buffer, the peaks of sample 1 were severely overlapped at the same concentration. The residual curves of the proposed method (Figure 5a,d) and TWOA (Figure 5b,e) had significantly less fluctuation than those of the LM algorithm (Figure 5c,f). This fluctuation is because the LM algorithm fits the ion signal to a large peak. Except for a few signal points, the fitted curve of the proposed method fits well to the bulk of the ion signal. The residual curves showed that the fitting accuracy of the proposed algorithm was close to that of the WOA algorithm, and both were higher than the LM algorithm.

Table 4 shows the number of fittings that regard the experimental data as a single peak over 100 fittings. In each fit, the proposed algorithm fitted the experimental data to two peaks. However, the LM algorithm often treated the experimental data as a single peak, especially for the detection signal of sample 1. Table 4 shows that the global optimization ability of the proposed algorithm was close to that of the TWOA algorithm. In contrast, for ion peaks with a large degree of overlap, the LM algorithm with an inappropriate starting point was likely to fall into a local minimum.

Table 4. The number of single peaks fitted to the experimental data.

Sample	TWOA	LM	TWOALM
NH_4^+&K^+	0	43	0
Ca^{2+}&Mg^{2+}	0	22	0

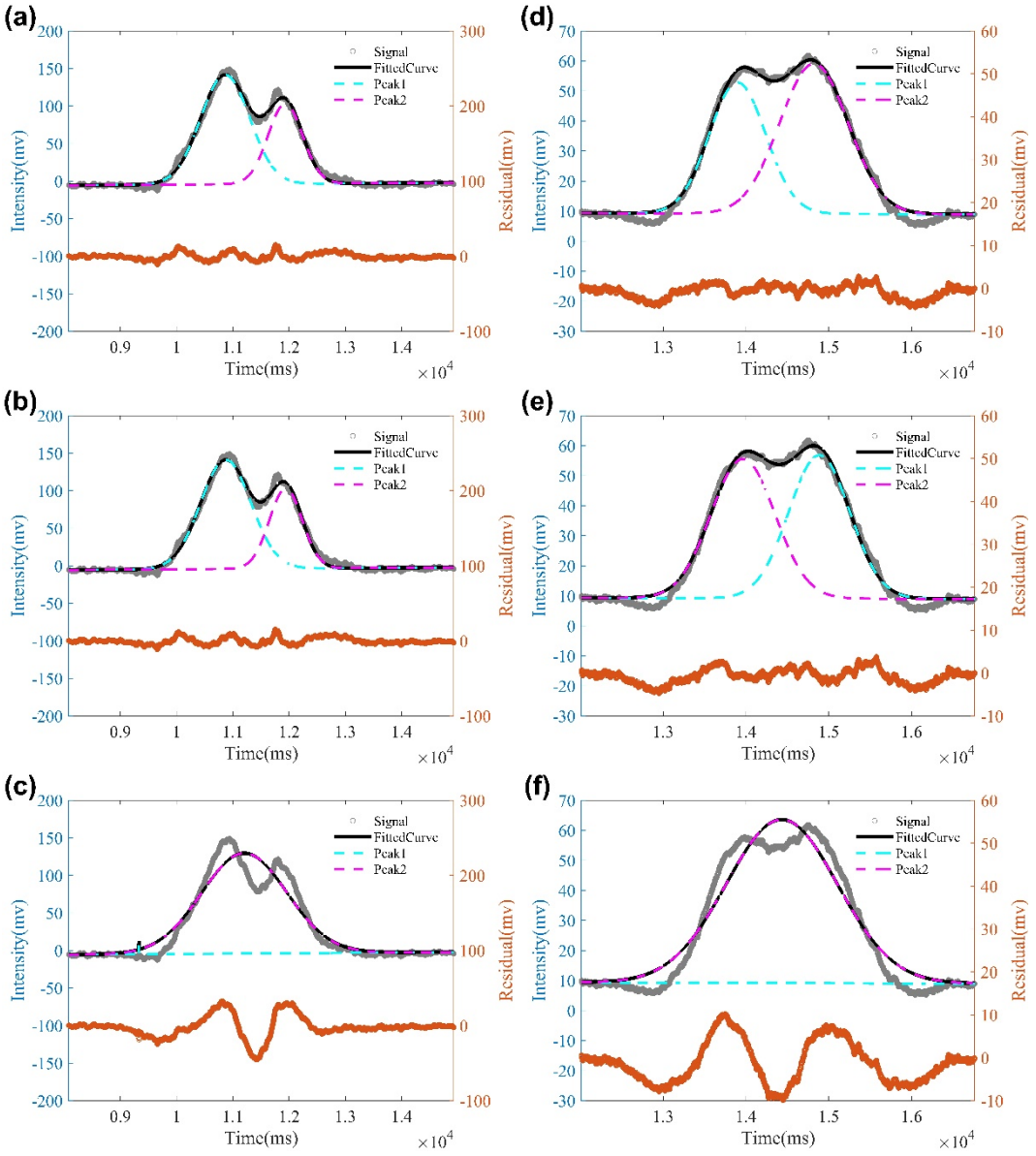

Figure 5. Fitting results of the experimental data. The subfigures (**a**–**c**) are the fitting results of the NH_4^+&K^+ signal, respectively. The subfigures (**d**–**f**) are the fitting results of the Ca^{2+}&Mg^{2+} signal, respectively. Experimental peaks, fitted peaks, peak 1 and peak 2 are represented by a grey circle, black solid line, cyan dashed line and magenta dashed line, respectively.

Table 5 shows the comparison of the fitting performance of the three algorithms to the experimental data. Table 5 shows that the proposed algorithm had the smallest fitting error, indicating that it can perform a more accurate analysis of the experimental data than other algorithms. In contrast, in terms of computational speed, both the proposed algorithm and the LM algorithm were significantly faster than the TWOA algorithm. The speeds of the proposed algorithm and the LM algorithm were close to each other. Moreover, by comparing the values of Error1 and Error2, it can be seen that the stability of the TWOALM algorithm was greater than that of LM. It can be seen from Table 5 that the computational speed of the proposed algorithm was significantly faster than that of the TWOA algorithm, which was consistent with the fitting results on synthetic data (Table 2). In contrast, the proposed algorithm can achieve higher fitting accuracy at a faster speed. In each calculation, the starting point of the LM algorithm was randomly generated. Hence, the fitting errors in Table 5 also show that the fitting performance of the LM algorithm is dependent on the

starting point. In contrast, the proposed algorithm can achieve higher fitting accuracy at a faster speed.

Table 5. Fitting error and calculation time of experimental data. Fitting errors are the mean (Error1) and median (Error2) of the RMSE over 100 fittings. The calculation time is the median time of 100 computations.

Sample		TWOA	LM	TWOALM
NH_4^+&K^+	Error1	4.099440085	8.303486631	**4.099440072**
	Error2	4.099440072	4.099440072	4.099440072
	Time(s)	32.6398813	0.21237084	**0.176207775**
Ca^{2+}&Mg^{2+}	Error1	1.589428358	2.298334751	**1.589428313**
	Error2	1.589428316	1.589428313	1.589428313
	Time(s)	29.06685794	0.155972324	**0.11844894**

A comprehensive analysis of the fitting results of synthetic peaks (Tables 2 and 3, Figures 3 and 4) and microchip electrophoresis ion peaks (Tables 4 and 5, Figure 5) showed that the proposed overlapping peak analysis algorithm combined the fitting accuracy of the TWOA algorithm and the convergence speed of the LM algorithm. The algorithm has great application prospects, not only for analyzing electrophoretic overlapping peaks, but also for processing high-throughput peak signals such as chromatography, spectroscopy and mass spectrometry.

6. Conclusions

In this article, we used a commonly used chaotic map method, tent map, to improve the WOA algorithm and propose the TWOA algorithm. Specifically, we used tent mapping to replace the uniformly distributed parameters in the original WOA, and then used simulation experiments to verify its convergence performance. In addition, we proposed a peak fitting algorithm TWOALM based on the proposed TWOA algorithm and the LM algorithm. Simulation peaks with different noise levels and resolutions and microchip electrophoresis experimental data were used to verify the performance of the algorithm. This algorithm effectively solves the dependence of the LM algorithm on the starting point and has broad application prospects. The fitting results of the simulated peaks and microchip electrophoresis ion peaks showed that the combination of the chaotic map-based WOA algorithm and LM algorithm could significantly improve the fitting accuracy of overlapping peaks. To expand the application of this method, more peak function fitting needs to be further studied in the future. In addition, the problem of multiple peaks overlapping, which is common in high-throughput signals, is worth further investigation. A feasible idea is to combine the peak detection method and expand it to quantitative analysis of three-dimensional overlapping signals.

Author Contributions: Writing—original draft preparation, W.H.; conceptualization—methodology, J.W. and Y.L. (Yaping Liu); methodology—validation, C.S.; writing—review and editing, Z.Q.; visualization, X.W.; project administration, Y.L. (Ying Liu); resources—funding acquisition, H.Y. All authors have read and agreed to the published version of the manuscript.

Funding: This research was funded by Key-Area Research and Development Program of Guangdong Province of China (Grant No. 2019B020219003), Guangxi Bagui Scholars Project (No. C3010099204) and the Interdisciplinary Scientific Research Foundation of GuangXi University (Grant No. 202200245).

Institutional Review Board Statement: Not applicable.

Informed Consent Statement: Not applicable.

Data Availability Statement: Not applicable.

Conflicts of Interest: The authors declare no conflict of interest.

Appendix A

In this section, the fitting results of different WOA algorithms for the synthetic peak with different SNRs are shown in Figures A1–A8, which are cited in the main text (Section 3.1).

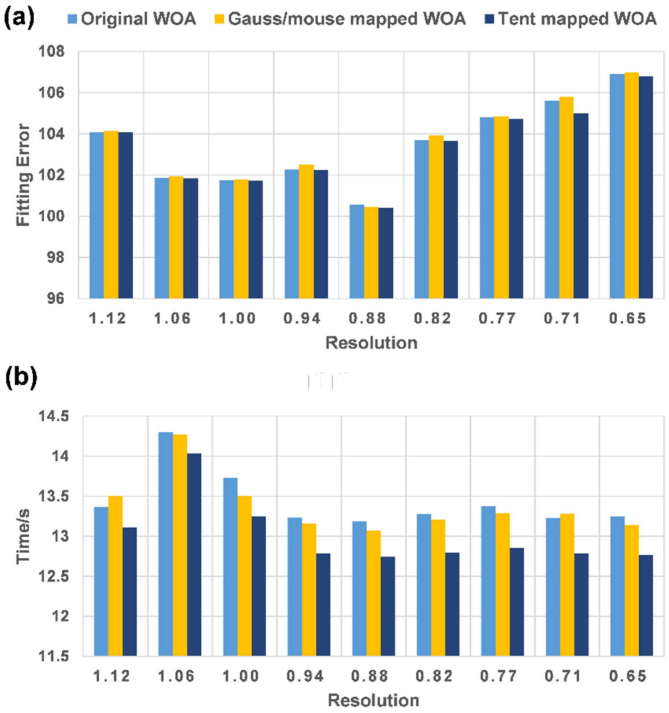

Figure A1. The fitting results of different WOA algorithms for the synthetic peak with SNR of 10 dB. (**a**) Fitting error (root mean square error), (**b**) calculation time (mean value).

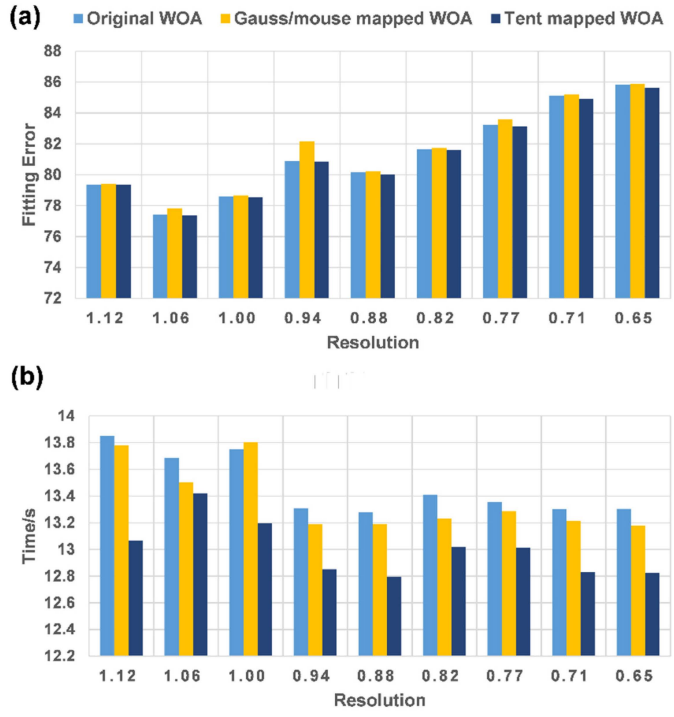

Figure A2. The fitting results of different WOA algorithms for the synthetic peak with SNR of 12 dB. (**a**) Fitting error (root mean square error), (**b**) calculation time (mean value).

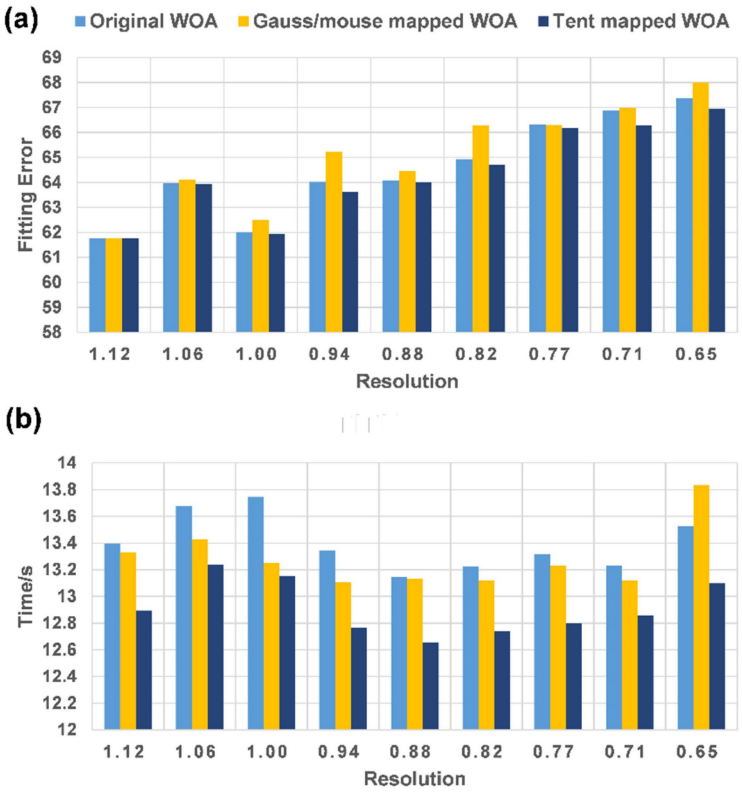

Figure A3. The fitting results of different WOA algorithms for the synthetic peak with SNR of 14 dB. (**a**) Fitting error (root mean square error), (**b**) calculation time (mean value).

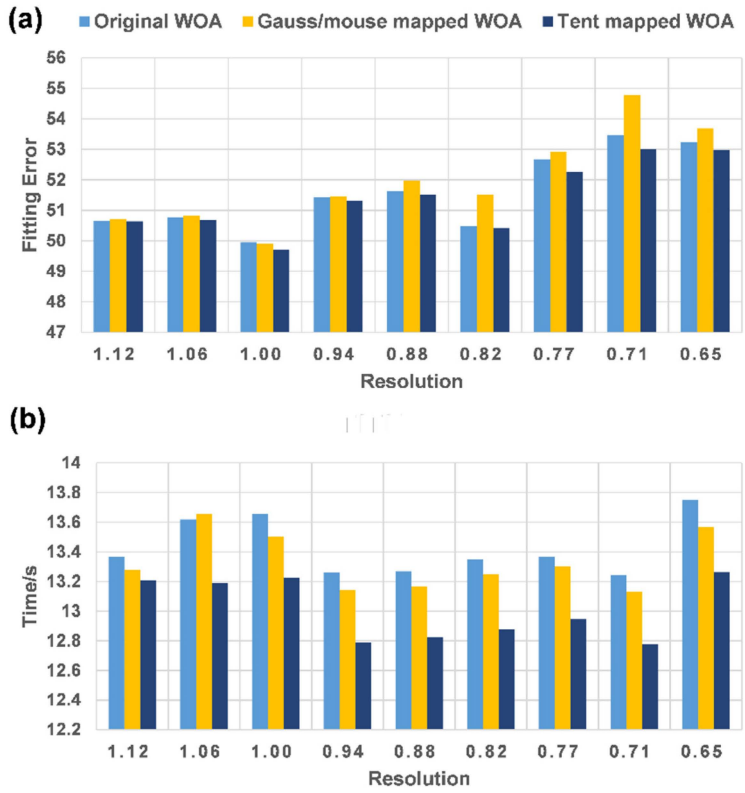

Figure A4. The fitting results of different WOA algorithms for the synthetic peak with SNR of 16 dB. (**a**) Fitting error (root mean square error), (**b**) calculation time (mean value).

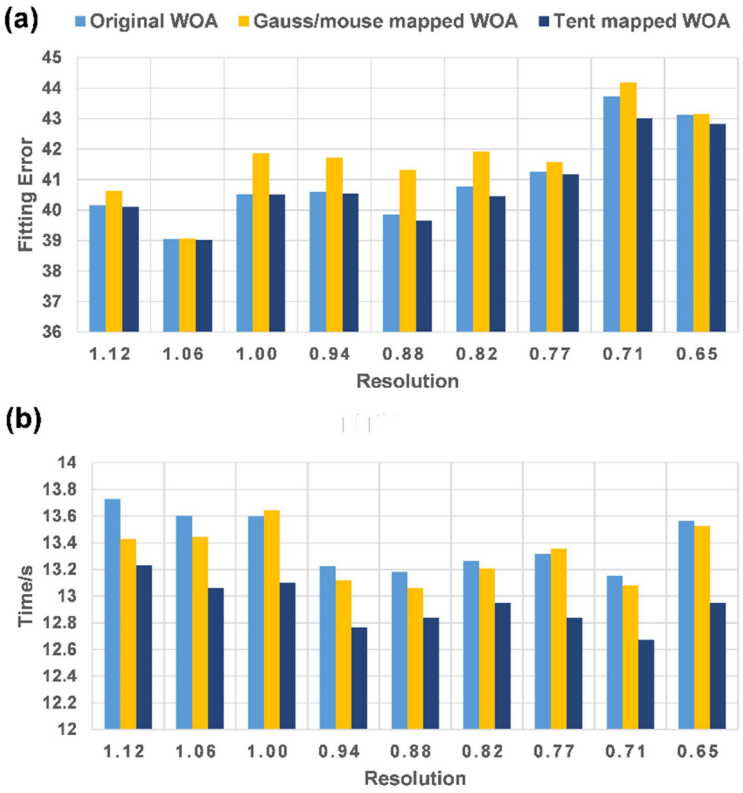

Figure A5. The fitting results of different WOA algorithms for the synthetic peak with SNR of 18 dB. (**a**) Fitting error (root mean square error), (**b**) calculation time (mean value).

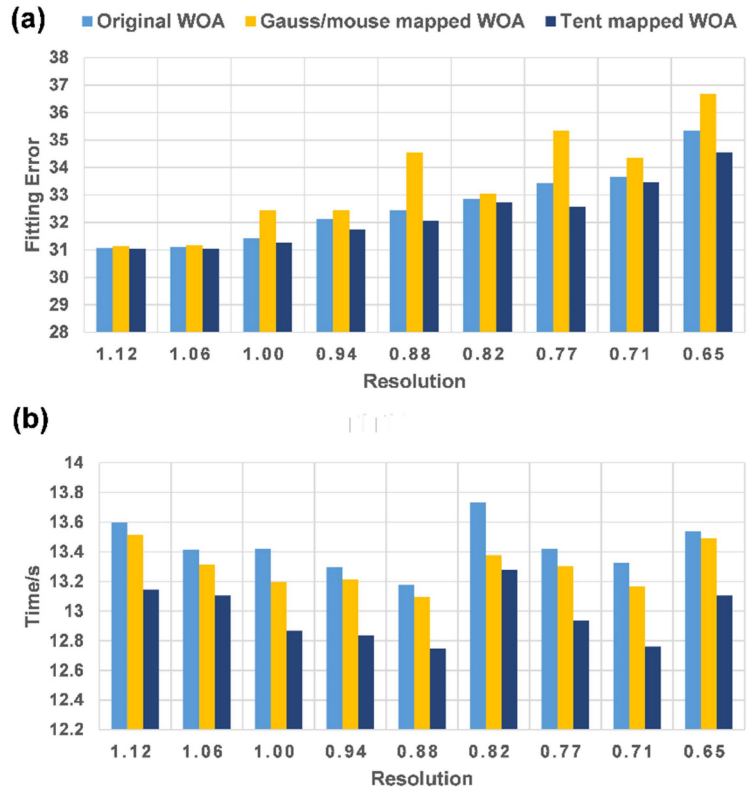

Figure A6. The fitting results of different WOA algorithms for the synthetic peak with SNR of 20 dB. (**a**) Fitting error (root mean square error), (**b**) calculation time (mean value).

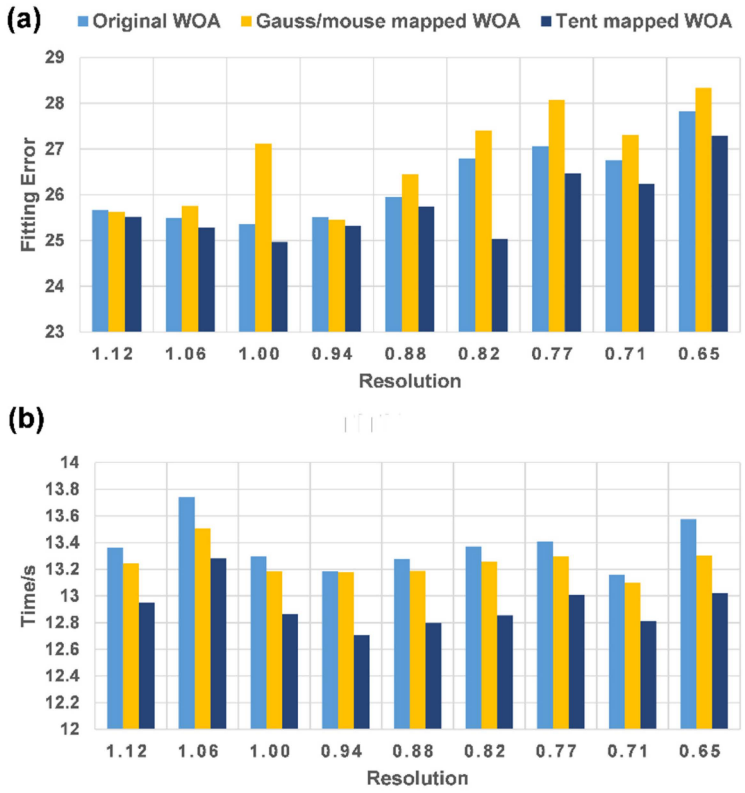

Figure A7. The fitting results of different WOA algorithms for the synthetic peak with SNR of 22 dB. (**a**) Fitting error (root mean square error), (**b**) calculation time (mean value).

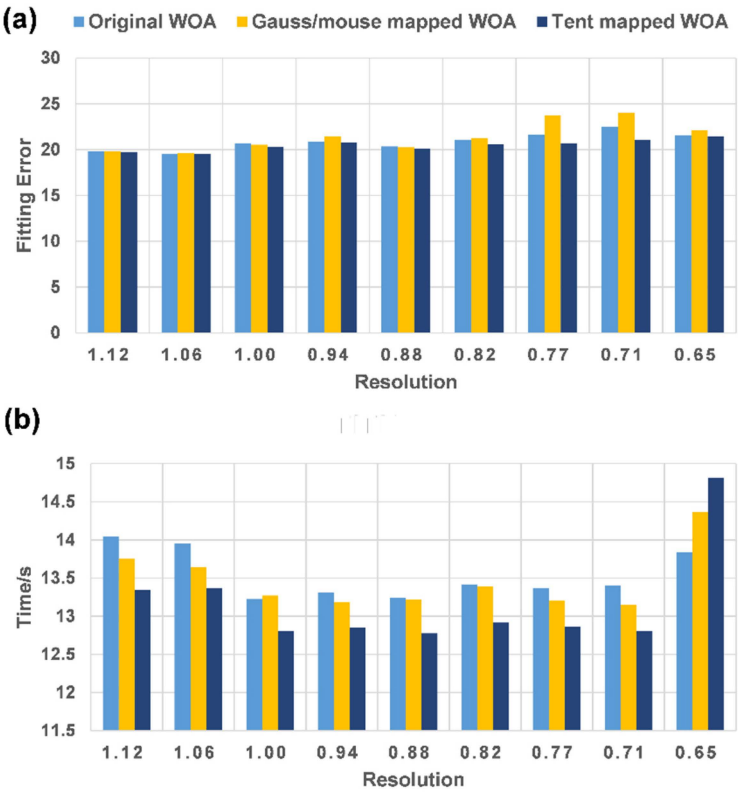

Figure A8. The fitting results of different WOA algorithms for the synthetic peak with SNR of 24 dB. (**a**) Fitting error (root mean square error), (**b**) calculation time (mean value).

References

1. Yang, M.P.; Huang, Z.; Xie, Y.; You, H. Development of Microchip Electrophoresis and Its Applications in Ion Detection. *Chin. J. Anal. Chem.* **2018**, *46*, 631–641. [CrossRef]
2. Nielsen, J.B.; Nielsen, A.V.; Carson, R.H.; Lin, H.J.L.; Hanson, R.L.; Sonker, M.; Mortensen, D.N.; Price, J.C.; Woolley, A.T. Analysis of thrombin-antithrombin complex formation using microchip electrophoresis and mass spectrometry. *Electrophoresis* **2019**, *40*, 2853–2859. [CrossRef]
3. Alatawi, H.; Hogan, A.; Albalawi, I.; O'Sullivan-Carroll, E.; Alsefri, S.; Wang, Y.; Moore, E. Rapid determination of NSAIDs by capillary and microchip electrophoresis with capacitively coupled contactless conductivity detection in wastewater. *Electrophoresis* **2022**, *43*, 1944–1952. [CrossRef] [PubMed]
4. Zhou, F.; Li, C.; Zhu, H.; Li, Y. A novel method for simultaneous determination of zinc, nickel, cobalt and copper based on UV–vis spectrometry. *Optik* **2019**, *182*, 58–64. [CrossRef]
5. Nilsson, M.L.; Bengtsson, S.; Kylin, H. Identification and determination of chlorinated paraffins using multivariate evaluation of gas chromatographic data. *Environ. Pollut.* **2012**, *163*, 142–148. [CrossRef]
6. Lv, X.; Wang, S.; Zhao, Y.; Shan, P. A reinforcement learning based method for protein's differential scanning calorimetry signal separation. *Meas. J. Int. Meas. Confed.* **2022**, *188*, 110391. [CrossRef]
7. Jamshidi, M.; Ghaedi, M.; Dashtian, K.; Ghaedi, A.M.; Hajati, S.; Goudarzi, A.; Alipanahpour, E. Highly efficient simultaneous ultrasonic assisted adsorption of brilliant green and eosin B onto ZnS nanoparticles loaded activated carbon: Artificial neural network modeling and central composite design optimization. *Spectrochim. Acta-Part A Mol. Biomol. Spectrosc.* **2016**, *153*, 257–267. [CrossRef]
8. Yang, G.; Dai, J.; Liu, X.; Chen, M.; Wu, X. Spectral feature extraction based on continuous wavelet transform and image segmentation for peak detection. *Anal. Methods* **2020**, *12*, 169–178. [CrossRef]
9. Hellinghausen, G.; Wahab, M.F.; Armstrong, D.W. Improving peak capacities over 100 in less than 60 seconds: Operating above normal peak capacity limits with signal processing. *Anal. Bioanal. Chem.* **2020**, *412*, 1925–1932. [CrossRef]
10. Liu, H.; Yan, L.; Huang, T.; Liu, S.; Zhang, Z. Blind Spectral Signal Deconvolution with Sparsity Regularization: An Iteratively Reweighted Least-Squares Solution. *Circuits Syst. Signal Process.* **2017**, *36*, 435–446. [CrossRef]
11. Wahab, M.F.; Gritti, F.; O'Haver, T.C.; Hellinghausen, G.; Armstrong, D.W. Power Law Approach as a Convenient Protocol for Improving Peak Shapes and Recovering Areas from Partially Resolved Peaks. *Chromatographia* **2019**, *82*, 211–220. [CrossRef]
12. Wahab, M.F.; O'Haver, T.C.; Gritti, F.; Hellinghausen, G.; Armstrong, D.W. Increasing chromatographic resolution of analytical signals using derivative enhancement approach. *Talanta* **2019**, *192*, 492–499. [CrossRef]
13. Marquardt, D.W. An Algorithm for Least-Squares Estimation of Nonlinear Parameters. *J. Soc. Ind. Appl. Math.* **1963**, *11*, 431–441. [CrossRef]
14. Fang, Q.; Zivanovic, R. Parameter identification of a wind generator unit RMS model using sparse grid optimization algorithm. In Proceedings of the 2014 International Conference on Modelling, Identification & Control, Melbourne, Australia, 3–5 December 2014; pp. 283–288. [CrossRef]
15. Fusco, R.; Sansone, M.; Petrillo, A. The Use of the Levenberg–Marquardt and Variable Projection Curve-Fitting Algorithm in Intravoxel Incoherent Motion Method for DW-MRI Data Analysis. *Appl. Magn. Reson.* **2015**, *46*, 551–558. [CrossRef]
16. Mariyappa, N.; Parasakthi, C.; Sengottuvel, S.; Gireesan, K.; Patel, R.; Janawadkar, M.P.; Sundar, C.S.; Radhakrishnan, T.S. Dipole location using SQUID based measurements: Application to magnetocardiography. *Phys. C Supercond. Its Appl.* **2012**, *477*, 15–19. [CrossRef]
17. Li, M.; Li, L.D. A Novel Method of Curve Fitting Based on Optimized Extreme Learning Machine. *Appl. Artif. Intell.* **2020**, *34*, 849–865. [CrossRef]
18. Mirjalili, S.; Lewis, A. The Whale Optimization Algorithm. *Adv. Eng. Softw.* **2016**, *95*, 51–67. [CrossRef]
19. Gharehchopogh, F.S.; Gholizadeh, H. A comprehensive survey: Whale Optimization Algorithm and its applications. *Swarm Evol. Comput.* **2019**, *48*, 1–24. [CrossRef]
20. Karakaplan, M.; Avcu, F.M. Deconvolution of Gaussian peaks with mixed real and discrete-integer optimization based on evolutionary computing. *J. Chemom.* **2020**, *34*, e3229. [CrossRef]
21. Lalu, M.; Phaneendra, K. Quadrature method with exponential fitting for delay differential equations having layer behavior. *J. Math. Comput. Sci.* **2021**, *25*, 191–208. [CrossRef]
22. Calabrese, I.; Merli, M.; Turco Liveri, M.L. Deconvolution procedure of the UV-vis spectra. A powerful tool for the estimation of the binding of a model drug to specific solubilisation loci of bio-compatible aqueous surfactant-forming micelle. *Spectrochim. Acta-Part A Mol. Biomol. Spectrosc.* **2015**, *142*, 150–158. [CrossRef] [PubMed]
23. Striegel, A.M.; Striegel, D.A. Peak Fraction Purity and Chromatographic Resolution: Gaussian Peaks Revisited. *Chromatographia* **2022**, *85*, 65–72. [CrossRef]
24. Wei, X.; Shi, X.; Kim, S.; Patrick, J.S.; Binkley, J.; Kong, M.; McClain, C.; Zhang, X. Data dependent peak model based spectrum deconvolution for analysis of high resolution LC-MS data. *Anal. Chem.* **2014**, *86*, 2156–2165. [CrossRef]
25. Xiong, J.; Liang, W.; Liang, X.; Zhang, M. An overlapping peak separation algorithm based on multiorder differential method and genetic algorithm for magnetic eddy current signal of a defect cluster. *Process. Saf. Prog.* **2020**, *39*, e12129. [CrossRef]
26. Henstridge, M.C.; Laborda, E.; Rees, N.V.; Compton, R.G. Marcus-Hush-Chidsey theory of electron transfer applied to voltammetry: A review. *Electrochim. Acta* **2012**, *84*, 12–20. [CrossRef]

27. Chen, G.Y.; Gan, M.; Wang, S.; Chen, C.L.P. Insights into Algorithms for Separable Nonlinear Least Squares Problems. *IEEE Trans. Image Process.* **2021**, *30*, 1207–1218. [CrossRef] [PubMed]
28. Sadygov, R.G.; Zhao, Y.; Haidacher, S.J.; Starkey, J.M.; Tilton, R.G.; Denner, L. Using power spectrum analysis to evaluate 18o-water labeling data acquired from low resolution mass spectrometers. *J. Proteome Res.* **2010**, *9*, 4306–4312. [CrossRef]
29. El-Shal, M.A.; Hendawy, H.A.M. Highly sensitive voltammetric sensor using carbon nanotube and an ionic liquid composite electrode for xylazine hydrochloride. *Anal. Sci.* **2019**, *35*, 189–194. [CrossRef]
30. Xu, J.; Zhu, L.; Xu, G.; Yu, W.; Ray, A.K. Determination of competitive adsorption isotherm of enantiomers on preparative chromatographic columns using inverse method. *J. Chromatogr. A* **2013**, *1273*, 49–56. [CrossRef]
31. James, T.M.; Schlösser, M.; Lewis, R.J.; Fischer, S.; Bornschein, B.; Telle, H.H. Automated quantitative spectroscopic analysis combining background subtraction, cosmic ray removal, and peak fitting. *Appl. Spectrosc.* **2013**, *67*, 949–959. [CrossRef]
32. Zhang, B.; Yu, H.; Sun, L.; Xin, Y.; Conga, Z. A method for resolving overlapped peaks in laser-induced breakdown spectroscopy (LIBS). *Appl. Spectrosc.* **2013**, *67*, 1087–1097. [CrossRef] [PubMed]
33. Song, F.; Wei, J.; Jiang, M.; Zhang, L.; Zhang, F.; Sui, Q.; Tian, Y.; Sun, W. The Optimization Study of FBG Gaussian Fitting Peak-Detection Based on Levenberg-Marquardt Algorithm. In Proceedings of the 2017 Chinese Automation Congress (CAC), Jinan, China, 20–22 October 2017; IEEE: Jinan, China, 2017; pp. 3723–3727.
34. Teng, Z.; Lv, J.; Guo, L. An improved hybrid grey wolf optimization algorithm. *Soft Comput.* **2019**, *23*, 6617–6631. [CrossRef]
35. Shaheen, M.A.M.; Hasanien, H.M.; El Moursi, M.S.; El-Fergany, A.A. Precise modeling of PEM fuel cell using improved chaotic MayFly optimization algorithm. *Int. J. Energy Res.* **2021**, *45*, 18754–18769. [CrossRef]
36. Sayed, G.I.; Tharwat, A.; Hassanien, A.E. Chaotic dragonfly algorithm: An improved metaheuristic algorithm for feature selection. *Appl. Intell.* **2019**, *49*, 188–205. [CrossRef]
37. Misaghi, M.; Yaghoobi, M. Improved invasive weed optimization algorithm (IWO) based on chaos theory for optimal design of PID controller. *J. Comput. Des. Eng.* **2019**, *6*, 284–295. [CrossRef]
38. Nikan, O.; Avazzadeh, Z. Coupling of the Crank–Nicolson scheme and localized meshless technique for viscoelastic wave model in fluid flow. *J. Comput. Appl. Math.* **2021**, *398*, 113695. [CrossRef]
39. Dvořák, M.; Svobodová, J.; Dubský, P.; Riesová, M.; Vigh, G.; Gaš, B. Equivalent peak resolution: Characterization of the extent of separation for two components based on their relative peak overlap. *Electrophoresis* **2015**, *36*, 646–654. [CrossRef]
40. Eftekhari Zadeh, E.; Feghhi, S.A.H.; Bayat, E.; Roshani, G.H. Gaussian Energy Broadening Function of an HPGe Detector in the Range of 40 keV to 1.46 MeV. *J. Exp. Phys.* **2014**, *2014*, 623683. [CrossRef]
41. Wang, J.; Liu, Y.; He, W.; Chen, Y.; You, H. A Novel Planar Grounded Capacitively Coupled Contactless Conductivity Detector for Microchip Electrophoresis. *Micromachines* **2022**, *13*, 394. [CrossRef]